Letter

Kekulé spirals and charge transfer cascades in twisted symmetric trilayer graphene

Ziwei Wang,[1] Yves H. Kwan,[2] Glenn Wagner,[3] Nick Bultinck,[1,4] Steven H. Simon,[1] and S. A. Parameswaran[1]
[1]*Rudolf Peierls Centre for Theoretical Physics, Parks Road, Oxford OX1 3PU, United Kingdom*
[2]*Princeton Center for Theoretical Science, Princeton University, Princeton, New Jersey 08544, USA*
[3]*Department of Physics, University of Zurich, Winterthurerstrasse 190, 8057 Zurich, Switzerland*
[4]*Department of Physics, Ghent University, Krijgslaan 281, 9000 Gent, Belgium*

(Received 2 February 2024; accepted 3 May 2024; published 16 May 2024)

We study the phase diagram of magic-angle twisted symmetric trilayer graphene in the presence of uniaxial heterostrain and interlayer displacement field. For experimentally reasonable strain, our mean-field analysis finds robust Kekulé spiral order whose doping-dependent ordering vector is incommensurate with the moiré superlattice, consistent with recent scanning tunneling microscopy experiments, and paralleling the behavior of closely related twisted bilayer graphene (TBG) systems. Strikingly, we identify a possibility absent in TBG: the existence of *commensurate* Kekulé spiral order even at zero strain for experimentally realistic values of the interlayer potential in a trilayer. Our studies also reveal a complex pattern of charge transfer between weakly and strongly dispersive bands in strained trilayer samples as the density is tuned by electrostatic gating, that can be understood intuitively in terms of the "cascades" in the compressibility of magic-angle TBG.

DOI: 10.1103/PhysRevB.109.L201119

Introduction. The discovery of superconductivity proximate to correlated insulating behavior [1–9] in twisted bilayer graphene (TBG) in the "magic-angle" regime [10,11] has stimulated intense investigation of a host of other multilayer graphene systems. Among these, alternating-twist multilayers exhibit identical moiré patterns between each pair of adjacent layers and have well-defined magic angles in the chiral limit [12]. The simplest member in the group, twisted symmetric trilayer graphene (TSTG), which is composed of three layers of graphene stacked together with the inner layer rotated, has been experimentally studied [13–25], especially in the context of its superconducting properties, and has received extensive theoretical investigation [26–52]. In the absence of external fields, the single-particle Hilbert space of TSTG can be decomposed into a direct sum of monolayer graphene and TBG parts [12], allowing many phenomena in TBG to be reproduced in TSTG. If one applies a perpendicular electric field, the TBG and graphene sectors are hybridized, allowing for further tunability of the system.

Among the various correlated states in TBG, a novel form of translation symmetry breaking order dubbed the incommensurate Kekulé spiral (IKS) has been proposed by some of us to characterize the many-body ground state at all integer fillings except charge neutrality [53], as well as a range of noninteger fillings [54]. The signature of the proposed state, which is stabilized by experimentally realistic uniaxial strains, consists of a graphene scale Kekulé-like pattern with complex spatial dependence on the moiré scale, and has recently been observed with high-resolution scanning tunneling microscopy (STM) [55]. A similar pattern has also been observed in TSTG [25], but Kekulé spiral order in TSTG is theoretically unexplored, motivating the present work.

Here, we perform extensive Hartree-Fock (HF) simulations of TSTG that incorporate the effect of strain and allow for translation symmetry breaking. As in the case of TBG, we find IKS to be ubiquitous for nonzero integer and noninteger fillings of TSTG at finite strain. Furthermore, we find that *commensurate* Kekulé spiral (CKS) order in unstrained TSTG can be accessed even at zero strain by applying a large interlayer potential—a possibility absent in TBG. These results should be contrasted with previous studies of TSTG [36,40,44,50,52] at zero strain. We also explore the process of "charge transfer" between the TBG and graphene sectors of TSTG at zero interlayer potential, and elucidate subtleties in defining commensurate fillings in light of this mechanism.

Model and symmetries. TSTG is made by stacking three sheets of graphene with the middle layer twisted by an angle θ relative to the top and bottom layers [Fig. 1(a)]. The moiré patterns generated within the top and bottom pairs of layers are identical, preserving the overall moiré periodicity of the system. The single-particle Hamiltonian of TSTG can be decomposed [12] into a mirror-symmetry even sector, which is effectively a renormalized version of TBG, and a mirror-symmetry odd sector, which resembles monolayer graphene [Fig. 1(b)]. The magic angles of TSTG and TBG are related via $\theta_{\mathrm{TSTG}} = \sqrt{2}\theta_{\mathrm{TBG}} \approx 1.56^\circ$. In contrast to TBG, an electric displacement field normal to the layers has a significant effect: It produces an interlayer potential that breaks the mirror symmetry and mixes the odd and even sectors [Fig. 1(c)]. This modifies the dispersion, expanding the parameter space for new phases.

We also incorporate the effect of uniaxial strain in the system. Homostrain (where all layers experience the same strain) has only a small effect on TBG [56], and we expect it

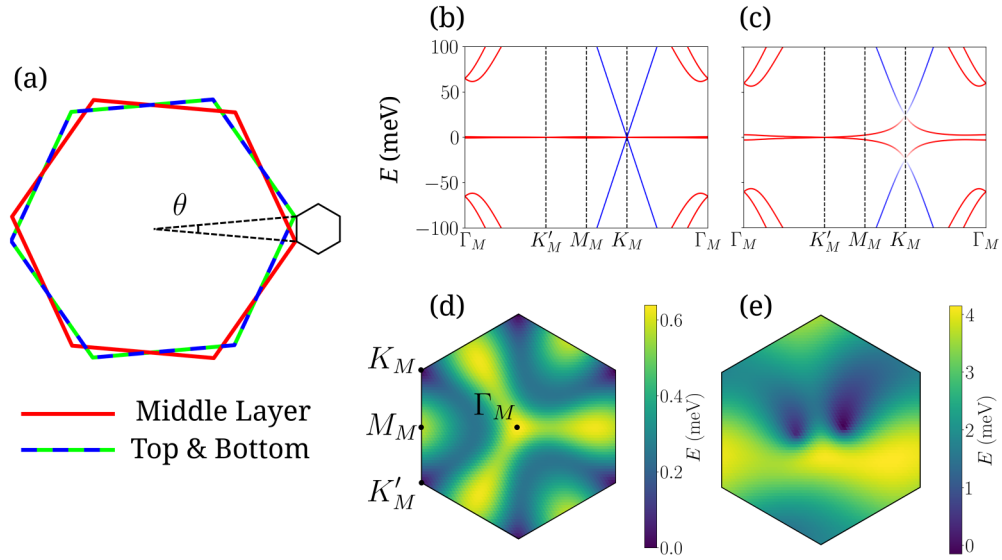

FIG. 1. Twisted symmetric trilayer graphene. (a) The large hexagons denote graphene Brillouin zones (BZs) of individual layers and the small hexagon denotes the moiré BZ for valley K. (b) Without interlayer potential, TSTG decomposes into a TBG sector (red) and a graphene sector (blue) with opposite mirror eigenvalues. (c) A finite interlayer potential (100 meV) breaks mirror symmetry and hybridizes the two sectors. The color represents the relative weight of the wave function on the zero-field TBG and graphene sectors. (d), (e) TBG sector conduction band at zero interlayer potential without and with strain ($\epsilon = 0.1\%$), respectively. Strain breaks C_3 symmetry, unpinning the Dirac points, and increases the bandwidth. The corresponding band structures in valley K' can be found using time-reversal symmetry.

to play a similarly minor role in TSTG. Therefore, we restrict our attention to heterostrain, produced by unequal strain in the different layers. In principle, strain could break the mirror symmetry of the system and introduce incommensurate moiré patterns for the top and bottom pairs of layers, potentially leading to a supermoiré pattern. However, we focus here on the case where top and bottom layers experience identical strains, thus preserving the moiré periodicity of the system. This choice can be justified as STM experiments observe well-defined moiré patterns in large regions of the TSTG samples [16,17,25]. We also ignore the small-angle Pauli-matrix rotations in the Dirac kinetic terms in each layer; then, absent strain or interlayer potential, the system has exact particle-hole symmetry, which is lost when both perturbations are included.

Phase diagram. We perform band-projected self-consistent HF calculations on the model discussed above at the magic angle $\theta = 1.56^\circ$. We use realistic hopping parameters $w_{\mathrm{AA}} = 75$ meV and $w_{\mathrm{AB}} = 110$ meV (the choice of $w_{\mathrm{AA}} < w_{\mathrm{AB}}$ takes into account of the effect of lattice relaxation in a phenomenological manner [57]), and include strain ϵ and interlayer potential ΔV as free parameters of the model. We model interactions via the dual-gate screened Coulomb potential $V(q) = (e^2/2\epsilon_0\epsilon_r q)\tanh qd$, with a screening length $d = 25$ nm and relative permittivity $\epsilon_r = 10$. To avoid double-counting interactions, we use the "average" subtraction scheme, detailed in the Supplemental Material [58] (see also Refs. [59–67] therein). Despite the lack of exact particle-hole symmetry for $\Delta V, \epsilon \neq 0$, we find that the phase diagrams at ν and $-\nu$ are qualitatively similar. Hence we only present results for $|\nu| \geqslant 0$ in the main text, and refer readers to the Supplemental Material [58] for $\nu < 0$ results.

Unless otherwise noted, we assume collinear spin configurations, but we have also checked that, for the parameter range in Fig. 2, relaxing this condition does not lead to different ground states up to $\mathrm{SU}(2)_K \times \mathrm{SU}(2)_{K'}$ valley-dependent spin rotations. In order to capture the incommensurate Kekulé spirals (IKS) proposed in Ref. [53] or its commensurate counterparts, we allow for coherence between states of momentum $\boldsymbol{k} - \tau\boldsymbol{q}/2$ in valley τ with states of momentum $\boldsymbol{k} - \tau'\boldsymbol{q}/2$ in valley τ' (here, τ and τ' take on values of ± 1) for some Kekulé spiral vector $\boldsymbol{q}$ in our HF calculations, and then optimize over all $\boldsymbol{q}$. One could further consider the slightly more general situation where the two spin sectors have different $\boldsymbol{q}$. As such, the one-particle density matrix takes the form

$$\left\langle \hat{c}^\dagger_{\boldsymbol{k}-\tau\boldsymbol{q}_s/2,\tau sa}\hat{c}_{\boldsymbol{k}-\tau'\boldsymbol{q}_s/2,\tau' sb}\right\rangle = P_{\tau a;\tau' b}(\boldsymbol{k}, s), \tag{1}$$

where s is the spin index, a and b are single-particle band indices, and $\boldsymbol{q}_s$ is the Kekulé spiral vector with possible spin dependence. In the majority of cases, this spin dependence is not relevant and we simply scan over $\boldsymbol{q}_\uparrow = \boldsymbol{q}_\downarrow \equiv \boldsymbol{q}$. The spin dependence of Kekulé spiral vectors becomes relevant when both spin sectors have intervalley coherence and the two sectors are nonequivalent, as is the case for $\nu = 1$. As such, we have allowed $\boldsymbol{q}_\uparrow \neq \boldsymbol{q}_\downarrow$ when computing the phase diagram at $\nu = 1$. For the range of interlayer potentials considered in the main text, we found that allowing for more generic translation symmetry breaking beyond Eq. (1) does not lead to different results. At higher interlayer potentials, we observe a complex pattern of translational symmetry breaking with nontrivial spin structure [58].

Figure 2 shows the phase diagrams for $\nu = 0, 1, 2, 3$. Kekulé states involve a nonzero Kekulé vector $\boldsymbol{q}$ and finite intervalley coherence. To diagnose the presence of these states and demonstrate their robustness, we show energy differences per unit cell between the lowest-energy $\boldsymbol{q} = \boldsymbol{0}$ solution and

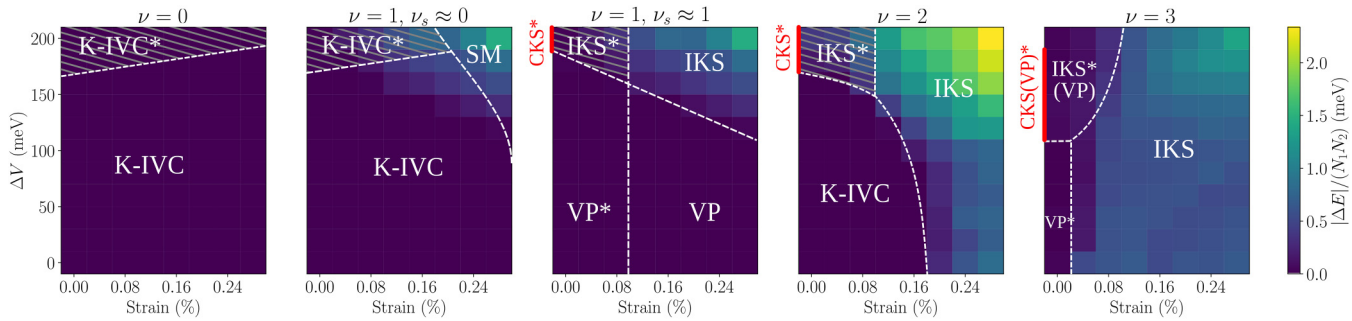

FIG. 2. Phase diagrams as a function of strain and interlayer potential at integer fillings ν. We have performed 10×10 self-consistent Hartree-Fock calculations, scanning over all possible Kekulé spiral vectors $\boldsymbol{q}$. ΔE is the energy difference per unit cell between the $\boldsymbol{q} = \boldsymbol{0}$ state with the overall energy minimum, and may be compared with temperature of a typical experiment in the field, which is of the order of 0.1 meV. The acronyms are K-IVC for Kramers-intervalley coherence, VP for valley polarization, (C/I)KS for (commensurate/incommensurate) Kekulé spiral, SM for (compensated) semimetal. An asterisk (*) denotes states that break C_2T symmetry. The (C/I)KS*(VP) region in $\nu = 3$ consists of Kekulé spiral states with possible finite valley polarization. The red lines on the zero-strain axis indicate *commensurate* Kekulé spirals. The shaded regions have a finite charge gap. For $\nu = 1$, we have shown the phases and charge gaps of the two spin sectors separately, where ν_s denotes the filling of each spin sector. As ΔE cannot be separately defined for each spin sector, the data are simply duplicated in the two plots of $\nu = 1$.

the energy achieved by minimizing over all $\boldsymbol{q}$: Nonzero values indicate Kekulé spiral ground states.

At zero interlayer potential, the single-particle Hamiltonian decomposes into mirror-symmetry even (TBG) and odd (graphene) sectors. For all fillings and strains examined here, we observe no spontaneous breaking of this symmetry, and the two sectors are only coupled by Hartree terms. Compared to pure TBG, the inclusion of the graphene sector can lead to "charge transfer cascades" from the TBG sector, discussed below, but otherwise the phase diagram is consistent with the corresponding one for TBG [53]. We find that IKS order appears at $\nu = 2, 3$ at finite strain (Fig. 2). While for the range of strains shown in Fig. 2 we find a Kramers intervalley-coherent (K-IVC) state at $\nu = 0, 1$, for larger strains the system transitions into IKS at $\nu = 1$ and a symmetric state at $\nu = 0$, again consistent with the situation in TBG.

A nonzero interlayer potential mixes the two symmetry sectors, and the simple picture of Hartree-coupled TBG and graphene sectors is no longer applicable. The mixing of relatively flat TBG bands with graphene bands leads to more dispersive central bands. This favors the formation of IKS by reducing the minimal strain required for its stabilization, except at charge neutrality, where no Kekulé spiral is observed for either TBG or TSTG.

At a high interlayer potential of about 200 meV, a common feature except at $\nu = 3$, is the breaking of C_2T symmetry and the opening of a charge gap. While strong C_2T breaking has not been observed in monolayer graphene under ordinary conditions, as graphene orbitals are hybridized with TBG orbitals, the Dirac point becomes less dispersive and interaction-induced spontaneous symmetry breaking becomes possible. For $\nu = 3$, C_2T symmetry only spontaneously breaks in one of the two spin sectors, leaving the system gapless. We note that Ref. [21] finds a charge gap at $\nu = 2$, in qualitative agreement with our result.

The phase diagram is most complex at $\nu = 1$, where the two spin sectors have densities of approximately 0 and 1 electron per unit cell relative to their respective charge neutrality points (finite but small charge transfers between the two sectors could occur). The two sectors are only coupled with a Hartree interaction, and otherwise exhibit their own physics. To capture the physics correctly, we allow for different Kekulé vectors for the two sectors [68]. In particular, we find ground states with K-IVC ($\boldsymbol{q}_\uparrow = \boldsymbol{0}$) in the spin sector at charge neutrality and IKS ($\boldsymbol{q}_\downarrow \neq \boldsymbol{0}$) in the other spin sector.

Commensurate Kekulé spirals. Another phase that we identify in TSTG is the commensurate Kekulé spiral (CKS*) [69] at high interlayer potential and zero strain. In CKS*, the spiral wave vector relates the K_M point of valley K where TBG and graphene hybridization is most prominent, to the Γ_M point of valley K' (i.e., $\boldsymbol{q} = \boldsymbol{k}_{\Gamma_M} - \boldsymbol{k}_{K_M}$). The resulting spiral order is commensurate with moiré periodicity, as $3\boldsymbol{q}$ is a moiré reciprocal lattice vector. We note that CKS* further differs from IKS in that it breaks C_2T symmetry. This is also true of other "starred" states, including the (C/I)KS* at $\nu = 1, 2, 3$. At zero strain all Kekulé spiral states have commensurate $\boldsymbol{q}$ (except $\nu = 3$ and large ΔV), but this commensurability is lost once any finite strain is introduced (though the graphene scale lock-in mechanism introduced in Ref. [25] may stabilize commensuration at finite strain). While CKS* is possible at all of $\nu = 1, 2, 3$, it is only robust (i.e., significant energy advantage over competing states) at $\nu = 2$, where it is the ground state up to about $\Delta V = 240$ meV.

Charge transfer cascades. At zero interlayer potential, the TBG and graphene sectors are coupled only by Hartree terms as the mirror symmetry is unbroken. While the total electron density is fixed, electronic charge could transfer nontrivially between the two sectors, as first noted in Ref. [36] at $\nu = 3$ and large chiral ratio. We now track this charge transfer mechanism across general fillings, and with finite strain. We use a HF interpolation scheme [36] to mitigate finite-size effects on the dispersion and hence more accurately compute the charge transfer.

Figure 3 shows the filling of the TBG sector ν_{TBG} as a function of total filling ν. We observe plateaus at integer values of ν_{TBG} near $\nu = 2$ and $\nu = 3$. This can be rationalized in terms of the formation of a correlated insulator with a finite charge gap in the TBG sector, such that injection of a small

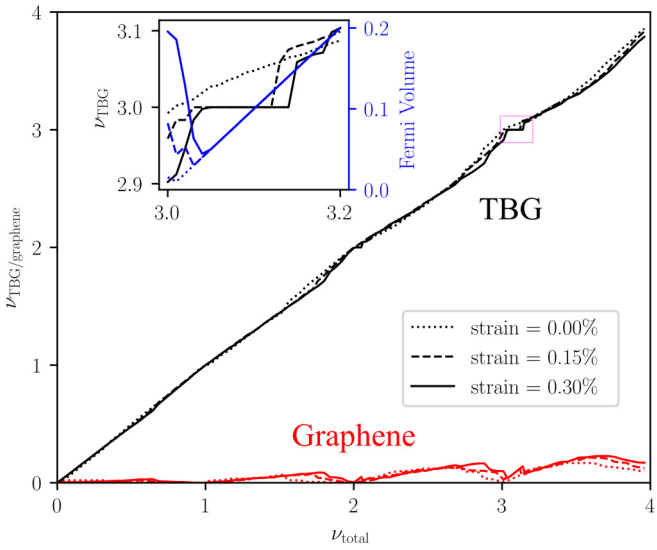

FIG. 3. "Charge transfer plateaus" in TSTG. We plot the fillings of TBG and graphene sectors from 10×10 self-consistent HF, interpolated to 60×60, as a function of total fillings. We notice plateaus at integer TBG fillings, which are due to a correlated charge gap in the TBG sector. In the inset, we additionally show the total unsigned Fermi volumes of all bands ("Fermi volume") as a measure of the metallicity of the system. We notice that, due to nontrivial charge transfer between the two sectors, minima in the Fermi volume need not occur exactly at total integer fillings.

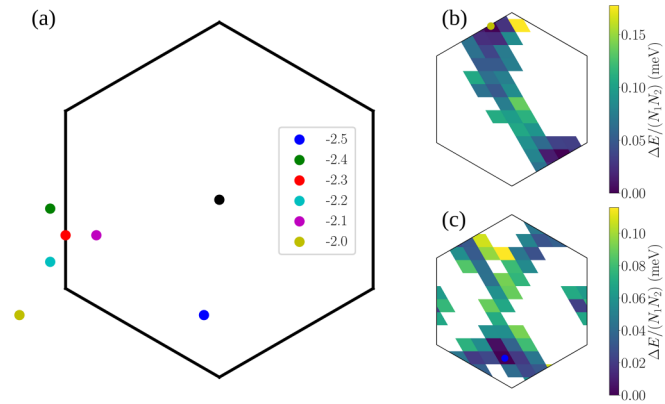

FIG. 4. (a) Doping-dependent $\boldsymbol{q}_{\text{Kekulé}}$ vectors, found from 10×10 HF, of a system with $\epsilon = -0.12\%$ and $\varphi = 87^\circ$, consistent with the experimental parameters in Ref. [25]. The hexagon [as well as the ones in (b) and (c)] represents the moiré Brillouin zone (mBZ), and $\boldsymbol{q}_{\text{Kekulé}}$ is only defined modulo mBZ. We set $\Delta V = 0$ as a displacement field in the single-gate geometry is weak, and use a single-gate screened Coulomb interaction $V(q) = (e^2/2\epsilon_0\epsilon_r q)(1 - e^{-2qd})$ with screening length $d = 25$ nm and relative permittivity $\epsilon_r = 20$. We take the middle-layer graphene to be rotated counterclockwise, as in experiment but opposite to our usual convention. (b), (c) $\boldsymbol{q}_{\text{Kekulé}}$ dependence of the energies of IKS states for $\nu = -2$ and $\nu = -2.5$, respectively, where $\Delta E = E(\boldsymbol{q}_{\text{Kekulé}}) - E_{\text{min}}$.

amount of additional charge only changes the filling in the graphene sector. The precise width of the plateau depends on the size of the TBG charge gap and the density of states of graphene at the chemical potential. We also find that the sum of unsigned Fermi volumes of all bands—a rough proxy for how "metallic" is the system—can reach a local minimum at noninteger total fillings, meaning that the most insulatorlike filling does not necessarily occur at integer ν due to the charge transfer.

In generating Fig. 3, we have determined the charge transfer from self-consistent HF calculations of the full system. However, if we treat the Hartree interaction between the two sectors as a function of only the densities of the respective sectors (which can be justified by assuming the graphene sector charge density is approximately uniform), we can write

$$E(n) = E_{\text{TBG}}(n_{\text{TBG}}) + E_{\text{graphene}}(n - n_{\text{TBG}}) + U_0 n_{\text{TBG}}(n - n_{\text{TBG}}), \tag{2}$$

where n denotes the total electron density and $U_0 = V(\boldsymbol{q} = \boldsymbol{0})$. We can rewrite this as

$$E(n) = \tilde{E}_{\text{TBG}}(n_{\text{TBG}}) + \tilde{E}_{\text{graphene}}(n - n_{\text{TBG}}), \tag{3}$$

where $\tilde{E}_{\text{TBG}}(n_{\text{TBG}}) = E_{\text{TBG}}(n_{\text{TBG}}) - U_0 n_{\text{TBG}}^2/2$ is the energy of the TBG sector with the electrostatic energy of uniform electron gas subtracted away, and similarly for $\tilde{E}_{\text{graphene}}$. We have also dropped terms that depend only on total electron density. Minimization of the total energy corresponds to $dE/dn_{\text{TBG}} = 0$, giving

$$\tilde{\mu}_{\text{TBG}} = \tilde{\mu}_{\text{graphene}}. \tag{4}$$

The graphene sector can be modeled as a noninteracting Dirac cone, so that we can estimate the charge transfer from the interacting physics of the TBG sector alone. The result is consistent with full TSTG HF calculations [58].

Comparison with experiments. Reference [25] observes Kekulé patterns using STM in a TSTG device with a heterostrain of $-(0.12 \pm 0.04)\%$ and finds doping-dependent $\boldsymbol{q}_{\text{Kekulé}}$ vectors, which are equivalent to our $\boldsymbol{q}$ vectors up to the choice of reference point, at fillings from -2 to -2.5. From our HF calculations with relative permittivity $\epsilon_r = 20$ (elsewhere in this Letter, $\epsilon_r = 10$; the effect of ϵ_r is discussed in the Supplemental Material [58]), at the experimental angle and magnitude of strain, we find that the ground states of TSTG for experimental parameters have IKS order, and we show the corresponding $\boldsymbol{q}_{\text{Kekulé}}$ in Fig. 4. We observe doping-dependent $\boldsymbol{q}_{\text{Kekulé}}$, in qualitative agreement with experiment. However, the values of $\boldsymbol{q}_{\text{Kekulé}}$ are highly sensitive to modeling details, and so we do not expect precise quantitative agreement.

Concluding remarks. Motivated by the experimental discovery of Kekulé spiral order in TSTG [25], we have systematically studied its ground state phase diagram under strain and interlayer potential. At zero interlayer potential, since the system decomposes into TBG and graphene sectors, the physics is similar to that of TBG, including the emergence of IKS order at finite strain. At finite interlayer potential, we find effects such as the breaking of C_2T symmetry and the formation of a commensurate Kekulé spiral state. Our prediction that the Kekulé spiral state at $\nu = 2$ breaks C_2T symmetry and opens up a charge gap is in agreement with experimental results [21]. The *commensurate* spiral state at zero strain is an addition to the family of Kekulé spiral states introduced by the discovery of the *incommensurate* Kekulé spiral, and hints at a broader relevance of KS order beyond

strained samples. While the high interlayer potential required to stabilize the phase in TSTG necessitates a dual-gate device, precluding the direct detection of its Kekulé pattern using STM, the mechanism behind the formation of CKS order is more general, and could emerge in other moiré systems, especially in cases where C_2 symmetry is broken explicitly [70]. We have further investigated the normal (nonsuperconducting) state of TSTG at noninteger fillings. We establish a charge transfer cascade mechanism between the TBG and graphene sectors in the absence of an interlayer potential, and show that this is consistent with a picture where the two sectors are coupled by Hartree interactions and the TBG sector density of states tracks that of standalone TBG. Notably, we find that integer fillings of the TBG sector and "maximally insulating" densities need not coincide with overall integer filling, which has implications for experimentally mapping the phase diagram of TSTG.

Acknowledgments. We thank Étienne Lantagne-Hurtubise for useful discussions about Ref. [25], and acknowledge support from EPSRC Grant No. EP/S020527/1, the European Research Council (ERC) under the European Union Horizon 2020 Research and Innovation Programme (Grant Agreement No. 804213-TMCS), and Leverhulme Trust International Professorship grant (No. LIP-202-014). G.W. acknowledges funding from the University of Zurich Postdoc Grant No. FK-23-134.

[1] Y. Cao, V. Fatemi, A. Demir, S. Fang, S. L. Tomarken, J. Y. Luo, J. D. Sanchez-Yamagishi, K. Watanabe, T. Taniguchi, E. Kaxiras, R. C. Ashoori, and P. Jarillo-Herrero, Correlated insulator behaviour at half-filling in magic-angle graphene superlattices, Nature (London) **556**, 80 (2018).

[2] Y. Cao, V. Fatemi, S. Fang, K. Watanabe, T. Taniguchi, E. Kaxiras, and P. Jarillo-Herrero, Unconventional superconductivity in magic-angle graphene superlattices, Nature (London) **556**, 43 (2018).

[3] M. Yankowitz, S. Chen, H. Polshyn, Y. Zhang, K. Watanabe, T. Taniguchi, D. Graf, A. F. Young, and C. R. Dean, Tuning superconductivity in twisted bilayer graphene, Science **363**, 1059 (2019).

[4] X. Lu, P. Stepanov, W. Yang, M. Xie, M. A. Aamir, I. Das, C. Urgell, K. Watanabe, T. Taniguchi, G. Zhang, A. Bachtold, A. H. MacDonald, and D. K. Efetov, Superconductors, orbital magnets and correlated states in magic-angle bilayer graphene, Nature (London) **574**, 653 (2019).

[5] P. Stepanov, I. Das, X. Lu, A. Fahimniya, K. Watanabe, T. Taniguchi, F. H. L. Koppens, J. Lischner, L. Levitov, and D. K. Efetov, Untying the insulating and superconducting orders in magic-angle graphene, Nature (London) **583**, 375 (2020).

[6] Y. Saito, J. Ge, K. Watanabe, T. Taniguchi, and A. F. Young, Independent superconductors and correlated insulators in twisted bilayer graphene, Nat. Phys. **16**, 926 (2020).

[7] H. S. Arora, R. Polski, Y. Zhang, A. Thomson, Y. Choi, H. Kim, Z. Lin, I. Z. Wilson, X. Xu, J.-H. Chu, K. Watanabe, T. Taniguchi, J. Alicea, and S. Nadj-Perge, Superconductivity in metallic twisted bilayer graphene stabilized by WSe_2, Nature (London) **583**, 379 (2020).

[8] Y. Cao, D. Rodan-Legrain, J. M. Park, N. F. Q. Yuan, K. Watanabe, T. Taniguchi, R. M. Fernandes, L. Fu, and P. Jarillo-Herrero, Nematicity and competing orders in superconducting magic-angle graphene, Science **372**, 264 (2021).

[9] M. Oh, K. P. Nuckolls, D. Wong, R. L. Lee, X. Liu, K. Watanabe, T. Taniguchi, and A. Yazdani, Evidence for unconventional superconductivity in twisted bilayer graphene, Nature (London) **600**, 240 (2021).

[10] R. Bistritzer and A. H. MacDonald, Moiré bands in twisted double-layer graphene, Proc. Natl. Acad. Sci. USA **108**, 12233 (2011).

[11] G. Tarnopolsky, A. J. Kruchkov, and A. Vishwanath, Origin of magic angles in twisted bilayer graphene, Phys. Rev. Lett. **122**, 106405 (2019).

[12] E. Khalaf, A. J. Kruchkov, G. Tarnopolsky, and A. Vishwanath, Magic angle hierarchy in twisted graphene multilayers, Phys. Rev. B **100**, 085109 (2019).

[13] J. M. Park, Y. Cao, K. Watanabe, T. Taniguchi, and P. Jarillo-Herrero, Tunable strongly coupled superconductivity in magic-angle twisted trilayer graphene, Nature (London) **590**, 249 (2021).

[14] Y. Zhang, R. Polski, C. Lewandowski, A. Thomson, Y. Peng, Y. Choi, H. Kim, K. Watanabe, T. Taniguchi, J. Alicea, F. von Oppen, G. Refael, and S. Nadj-Perge, Promotion of superconductivity in magic-angle graphene multilayers, Science **377**, 1538 (2022).

[15] Y. Cao, J. M. Park, K. Watanabe, T. Taniguchi, and P. Jarillo-Herrero, Pauli-limit violation and re-entrant superconductivity in moiré graphene, Nature (London) **595**, 526 (2021).

[16] H. Kim, Y. Choi, C. Lewandowski, A. Thomson, Y. Zhang, R. Polski, K. Watanabe, T. Taniguchi, J. Alicea, and S. Nadj-Perge, Evidence for unconventional superconductivity in twisted trilayer graphene, Nature (London) **606**, 494 (2022).

[17] S. Turkel, J. Swann, Z. Zhu, M. Christos, K. Watanabe, T. Taniguchi, S. Sachdev, M. S. Scheurer, E. Kaxiras, C. R. Dean, and A. N. Pasupathy, Orderly disorder in magic-angle twisted trilayer graphene, Science **376**, 193 (2022).

[18] N. J. Zhang, Y. Wang, K. Watanabe, T. Taniguchi, O. Vafek, and J. I. A. Li, Electronic anisotropy in magic-angle twisted trilayer graphene, arXiv:2211.01352.

[19] S.-J. Yang, J.-H. Jung, E. Lee, E. Han, M.-Y. Choi, D. Jung, S. Choi, J.-H. Park, D. Oh, S. Noh, K.-J. Kim, P. Y. Huang, C.-C. Hwang, and C.-J. Kim, Wafer-scale programmed assembly of one-atom-thick crystals, Nano Lett. **22**, 1518 (2022).

[20] Z. Hao, A. M. Zimmerman, P. Ledwith, E. Khalaf, D. H. Najafabadi, K. Watanabe, T. Taniguchi, A. Vishwanath, and P. Kim, Electric field– tunable superconductivity in alternating-twist magic-angle trilayer graphene, Science **371**, 1133 (2021).

[21] C. Shen, P. J. Ledwith, K. Watanabe, T. Taniguchi, E. Khalaf, A. Vishwanath, and D. K. Efetov, Dirac spectroscopy of strongly correlated phases in twisted trilayer graphene, Nat. Mater. **22**, 316 (2023).

[22] X. Liu, N. J. Zhang, K. Watanabe, T. Taniguchi, and J. I. A. Li, Isospin order in superconducting magic-angle twisted trilayer graphene, Nat. Phys. **18**, 522 (2022).
[23] J.-X. Lin, P. Siriviboon, H. D. Scammell, S. Liu, D. Rhodes, K. Watanabe, T. Taniguchi, J. Hone, M. S. Scheurer, and J. I. A. Li, Zero-field superconducting diode effect in small-twist-angle trilayer graphene, Nat. Phys. **18**, 1221 (2022).
[24] Y. Li, S. Zhang, F. Chen, L. Wei, Z. Zhang, H. Xiao, H. Gao, M. Chen, S. Liang, D. Pei, L. Xu, K. Watanabe, T. Taniguchi, L. Yang, F. Miao, J. Liu, B. Cheng, M. Wang, Y. Chen, and Z. Liu, Observation of coexisting Dirac bands and moiré flat bands in magic-angle twisted trilayer graphene, Adv. Mater. **34**, 2205996 (2022).
[25] H. Kim, Y. Choi, É. Lantagne-Hurtubise, C. Lewandowski, A. Thomson, L. Kong, H. Zhou, E. Baum, Y. Zhang, L. Holleis, K. Watanabe, T. Taniguchi, A. F. Young, J. Alicea, and S. Nadj-Perge, Imaging inter-valley coherent order in magic-angle twisted trilayer graphene, Nature (London) **623**, 942 (2023).
[26] X. Li, F. Wu, and A. H. MacDonald, Electronic structure of single-twist trilayer graphene, arXiv:1907.12338.
[27] S. Carr, C. Li, Z. Zhu, E. Kaxiras, S. Sachdev, and A. Kruchkov, Ultraheavy and ultrarelativistic Dirac quasiparticles in sandwiched graphenes, Nano Lett. **20**, 3030 (2020).
[28] G. A. Tritsaris, S. Carr, Z. Zhu, Y. Xie, S. B. Torrisi, J. Tang, M. Mattheakis, D. T. Larson, and E. Kaxiras, Electronic structure calculations of twisted multi-layer graphene superlattices, 2D Mater. **7**, 035028 (2020).
[29] A. Lopez-Bezanilla and J. L. Lado, Electrical band flattening, valley flux, and superconductivity in twisted trilayer graphene, Phys. Rev. Res. **2**, 033357 (2020).
[30] Z. Wu, Z. Zhan, and S. Yuan, Lattice relaxation, mirror symmetry and magnetic field effects on ultraflat bands in twisted trilayer graphene, Sci. China: Phys., Mech. Astron. **64**, 267811 (2021).
[31] D. Călugăru, F. Xie, Z.-D. Song, B. Lian, N. Regnault, and B. A. Bernevig, Twisted symmetric trilayer graphene: Single-particle and many-body Hamiltonians and hidden nonlocal symmetries of trilayer moiré systems with and without displacement field, Phys. Rev. B **103**, 195411 (2021).
[32] J. Shin, B. L. Chittari, and J. Jung, Stacking and gate-tunable topological flat bands, gaps, and anisotropic strip patterns in twisted trilayer graphene, Phys. Rev. B **104**, 045413 (2021).
[33] C. Lei, L. Linhart, W. Qin, F. Libisch, and A. H. MacDonald, Mirror symmetry breaking and lateral stacking shifts in twisted trilayer graphene, Phys. Rev. B **104**, 035139 (2021).
[34] W. Qin and A. H. MacDonald, In-plane critical magnetic fields in magic-angle twisted trilayer graphene, Phys. Rev. Lett. **127**, 097001 (2021).
[35] V. T. Phong, P. A. Pantaleón, T. Cea, and F. Guinea, Band structure and superconductivity in twisted trilayer graphene, Phys. Rev. B **104**, L121116 (2021).
[36] F. Xie, N. Regnault, D. Călugăru, B. A. Bernevig, and B. Lian, Twisted symmetric trilayer graphene. II. Projected Hartree-Fock study, Phys. Rev. B **104**, 115167 (2021).
[37] Y. W. Choi and H. J. Choi, Dichotomy of electron-phonon coupling in graphene moiré flat bands, Phys. Rev. Lett. **127**, 167001 (2021).
[38] Z. Wu, X. Kuang, Z. Zhan, and S. Yuan, Magic angle and plasmon mode engineering in twisted trilayer graphene with pressure, Phys. Rev. B **104**, 205104 (2021).
[39] E. Lake and T. Senthil, Reentrant superconductivity through a quantum Lifshitz transition in twisted trilayer graphene, Phys. Rev. B **104**, 174505 (2021).
[40] P. J. Ledwith, E. Khalaf, Z. Zhu, S. Carr, E. Kaxiras, and A. Vishwanath, TB or not TB? Contrasting properties of twisted bilayer graphene and the alternating twist n-layer structures ($n = 3, 4, 5, \ldots$), arXiv:2111.11060.
[41] A. Fischer, Z. A. H. Goodwin, A. A. Mostofi, J. Lischner, D. M. Kennes, and L. Klebl, Unconventional superconductivity in magic-angle twisted trilayer graphene, npj Quantum Mater. **7**, 5 (2022).
[42] D. Guerci, P. Simon, and C. Mora, Higher-order Van Hove singularity in magic-angle twisted trilayer graphene, Phys. Rev. Res. **4**, L012013 (2022).
[43] H. D. Scammell, J. I. A. Li, and M. S. Scheurer, Theory of zero-field superconducting diode effect in twisted trilayer graphene, 2D Mater. **9**, 025027 (2022).
[44] M. Christos, S. Sachdev, and M. S. Scheurer, Correlated insulators, semimetals, and superconductivity in twisted trilayer graphene, Phys. Rev. X **12**, 021018 (2022).
[45] B. Xie, R. Peng, S. Zhang, and J. Liu, Alternating twisted multilayer graphene: Generic partition rules, double flat bands, and orbital magnetoelectric effect, npj Comput. Mater. **8**, 110 (2022).
[46] L. Classen, J. H. Pixley, and E. J. König, Interaction-induced velocity renormalization in magic-angle twisted multilayer graphene, 2D Mater. **9**, 031001 (2022).
[47] N. Leconte, Y. Park, J. An, A. Samudrala, and J. Jung, Electronic structure of lattice relaxed alternating twist tNG-multilayer graphene: From few layers to bulk AT-graphite, 2D Mater. **9**, 044002 (2022).
[48] X. Lin, C. Li, K. Su, and J. Ni, Energetic stability and spatial inhomogeneity in the local electronic structure of relaxed twisted trilayer graphene, Phys. Rev. B **106**, 075423 (2022).
[49] R. Samajdar, Y. Teng, and M. S. Scheurer, Moiré phonons and impact of electronic symmetry breaking in twisted trilayer graphene, Phys. Rev. B **106**, L201403 (2022).
[50] J. González and T. Stauber, Ising superconductivity induced from spin-selective valley symmetry breaking in twisted trilayer graphene, Nat. Commun. **14**, 2746 (2023).
[51] K. Shin, Y. Jang, J. Shin, J. Jung, and H. Min, Electronic structure of biased alternating-twist multilayer graphene, Phys. Rev. B **107**, 245139 (2023).
[52] J. Yu, M. Xie, B. A. Bernevig, and S. Das Sarma, Magic-angle twisted symmetric trilayer graphene as a topological heavy-fermion problem, Phys. Rev. B **108**, 035129 (2023).
[53] Y. H. Kwan, G. Wagner, T. Soejima, M. P. Zaletel, S. H. Simon, S. A. Parameswaran, and N. Bultinck, Kekulé spiral order at all nonzero integer fillings in twisted bilayer graphene, Phys. Rev. X **11**, 041063 (2021).
[54] G. Wagner, Y. H. Kwan, N. Bultinck, S. H. Simon, and S. A. Parameswaran, Global phase diagram of the normal state of twisted bilayer graphene, Phys. Rev. Lett. **128**, 156401 (2022).
[55] K. P. Nuckolls, R. L. Lee, M. Oh, D. Wong, T. Soejima, J. P. Hong, D. Călugăru, J. Herzog-Arbeitman, B. A. Bernevig, K. Watanabe, T. Taniguchi, N. Regnault, M. P. Zaletel, and A. Yazdani, Quantum textures of the many-body wavefunctions in magic-angle graphene, Nature (London) **620**, 525 (2023).
[56] L. Huder, A. Artaud, T. Le Quang, G. T. de Laissardière, A. G. M. Jansen, G. Lapertot, C. Chapelier, and V. T. Renard,

Electronic spectrum of twisted graphene layers under heterostrain, Phys. Rev. Lett. **120**, 156405 (2018).

[57] S. Carr, S. Fang, Z. Zhu, and E. Kaxiras, Exact continuum model for low-energy electronic states of twisted bilayer graphene, Phys. Rev. Res. **1**, 013001 (2019).

[58] See Supplemental Material at http://link.aps.org/supplemental/10.1103/PhysRevB.109.L201119 for phase diagrams at negative fillings, a comparison of different methods in calculating charge transfer, and other additional results.

[59] E. Cancès and C. Le Bris, Can we outperform the DIIS approach for electronic structure calculations? Int. J. Quantum Chem. **79**, 82 (2000).

[60] D. E. Parker, T. Soejima, J. Hauschild, M. P. Zaletel, and N. Bultinck, Strain-induced quantum phase transitions in magic-angle graphene, Phys. Rev. Lett. **127**, 027601 (2021).

[61] Z. Bi, N. F. Q. Yuan, and L. Fu, Designing flat bands by strain, Phys. Rev. B **100**, 035448 (2019).

[62] A. Blason and M. Fabrizio, Local Kekulé distortion turns twisted bilayer graphene into topological Mott insulators and superconductors, Phys. Rev. B **106**, 235112 (2022).

[63] J. Ingham, T. Li, M. S. Scheurer, and H. D. Scammell, Quadratic Dirac fermions and the competition of ordered states in twisted bilayer graphene, arXiv:2308.00748.

[64] H. Suzuura and T. Ando, Phonons and electron-phonon scattering in carbon nanotubes, Phys. Rev. B **65**, 235412 (2002).

[65] N. Bultinck, E. Khalaf, S. Liu, S. Chatterjee, A. Vishwanath, and M. P. Zaletel, Ground state and hidden symmetry of magic-angle graphene at even integer filling, Phys. Rev. X **10**, 031034 (2020).

[66] D. Călugăru, N. Regnault, M. Oh, K. P. Nuckolls, D. Wong, R. L. Lee, A. Yazdani, O. Vafek, and B. A. Bernevig, Spectroscopy of twisted bilayer graphene correlated insulators, Phys. Rev. Lett. **129**, 117602 (2022).

[67] J. P. Hong, T. Soejima, and M. P. Zaletel, Detecting symmetry breaking in magic angle graphene using scanning tunneling microscopy, Phys. Rev. Lett. **129**, 147001 (2022).

[68] For numerical efficiency we fix one spin sector to have $\boldsymbol{q} = \mathbf{0}$ as we observe no Kekulé spirals at $\nu = 0$. We have also performed HF allowing for most general symmetry breaking to confirm the adequacy of the method.

[69] The asterisk emphasizes C_2T-symmetry breaking, though in TSTG we do not find C_2T-conserving commensurate Kekulé spiral states.

[70] Y. H. Kwan, P. J. Ledwith, Chiu Fan Bowen Lo, and T. Devakul, Strong-coupling topological states and phase transitions in helical trilayer graphene, Phys. Rev. B **109**, 125141 (2024).